





Article

Green Synthesis of ZnO Nanoparticles Using *Licania tomentosa* Benth (Oiti) Leaf Extract: Characterization and Applications for the Photocatalytic Degradation of Crystal Violet Dye

Moudo Thiam ¹ , Aparecido de Jesus Bernardo ¹, Vanessa de Oliveira Arnoldi Pellegrini ¹, João Fernando Possatto ¹, Zolile Wiseman Dlamini ² , Tebogo Sfiso Mahule ³, Balla Diop Ngom ⁴, Belda Q. Mosepele ⁵, Force Tefo Thema ⁵ , Bhekile B. Mamba ⁶, Sreedevi Vallabhapurapu ⁷, Vijaya Srinivasu Vallabhapurapu ³ and Igor Polikarpov ^{1,*} 

¹ São Carlos Institute of Physics, University of São Paulo, Campus 2, Avenida Joo Dagnone, 1100, Jardim Santa Angelina, São Carlos 13563-120, Brazil; moudothiam_167@usp.br (M.T.); ajbernardo@usp.br (A.d.J.B.); varnoldi@yahoo.com.br (V.d.O.A.P.); possatto@usp.br (J.F.P.)

² Maths, Science and Technology Education, Central University of Technology, 20 President Brand Street, Bloemfontein 9300, South Africa; zdlamini@cut.ac.za

³ Physics Department, University of South Africa, 28 Pioneer Avenue, Florida Park, Johannesburg 1710, South Africa; mahults@unisa.ac.za (T.S.M.); vallavs@unisa.ac.za (V.S.V.)

⁴ Laboratoire de Photonique Quantique, Energie & NanoFabrication, Faculté des Sciences et Techniques, Université Cheikh Anta Diop de Dakar (UCAD), Dakar-Fann Dakar B.P. 5005, Senegal; balla.ngom@ucad.edu.sn

⁵ Botswana University of Agriculture and Natural Resources (BUAN), Private bag 0027, Gaborone, Botswana; bmosepele@buan.ac.bw (B.Q.M.); fthema@buan.ac.bw (F.T.T.)

⁶ Institute for Nanotechnology and Water Sustainability, College of Science, Engineering and Technology, University of South Africa, Private Bag X6, Florida, Johannesburg 1709, South Africa; mambabb@unisa.ac.za

⁷ School of Computing, University of South Africa, 28 Pioneer Avenue, Florida Park, Gauteng 1710, South Africa; vallas@unisa.ac.za

* Correspondence: ipolikarpov@ifsc.usp.br



Academic Editor: Christos Argiris

Received: 13 January 2025

Revised: 20 February 2025

Accepted: 6 March 2025

Published: 17 March 2025

Citation: Thiam, M.; Bernardo, A.d.J.; Pellegrini, V.d.O.A.; Possatto, J.F.; Dlamini, Z.W.; Mahule, T.S.; Ngom, B.D.; Mosepele, B.Q.; Thema, F.T.; Mamba, B.B.; et al. Green Synthesis of ZnO Nanoparticles Using *Licania tomentosa* Benth (Oiti) Leaf Extract: Characterization and Applications for the Photocatalytic Degradation of Crystal Violet Dye. *Processes* **2025**, *13*, 880. <https://doi.org/10.3390/pr13030880>

Copyright: © 2025 by the authors. Licensee MDPI, Basel, Switzerland. This article is an open access article distributed under the terms and conditions of the Creative Commons Attribution (CC BY) license (<https://creativecommons.org/licenses/by/4.0/>).

Abstract: Efficient plant biomass utilization is a key component in advancing a sustainable and circular bioeconomy. ZnO nanoparticle synthesis using plant extracts is actively studied as a part of this effort. Here, green ZnO nanoparticles were prepared using *Licania tomentosa* Benth (also known as Oiti) leaf extract. Characterization of the produced green ZnO nanoparticles (NPs) involved X-ray diffraction (XRD), scanning electron microscopy (SEM), energy-dispersive X-ray spectroscopy (EDS), Fourier transform infrared spectroscopy (FTIR) and UV–Visible spectroscopy (UV–Vis) techniques. Furthermore, we investigated photocatalytic degradation of the crystal violet (CV) dye catalyzed by the obtained ZnO NPs and evaluated the efficiency of the photodegradation process. The synthesized nanoparticles have an average crystallite size of 12.4 nm, as measured by XRD and have a spherical shape as revealed by SEM. UV–Vis studies show that ZnO nanoparticles have a relatively small band gap of 2.75 eV, as estimated by Tauc plot. The photodegradation activity tests using synthesized green ZnO NPs showed that approximately 79% of CV dye is decomposed in 2 h after being exposed to UV irradiation under experimentally studied conditions. The photodecomposition of CV is impacted by different factors, such as the catalyst bandgap and loading, the pH and the intensity of light. Moreover, an optimum photocatalyst loading was determined. Our studies reveal that Oiti leaf extract can be efficiently used for ZnO NPs synthesis, which has significant potential for photodegradation applications.

Keywords: ZnO nanoparticles; green synthesis; plant extracts; *Licania tomentosa* Benth (Oiti); photocatalytic degradation

1. Introduction

The building of sustainable and circular bioeconomy crucially depends on the wholistic use of plant biomass and available agricultural residues. While the main fractions of plant biomass (cellulose, hemicellulose and lignin) find numerous applications, e.g., for cellulosic ethanol, prebiotics and green chemical productions, the utilization of extractives from plant residues and agro-industrial side-streams deserve further investigation. One of the possible applications of plant extractives is in the sustainable green synthesis of different metal nanoparticles (NPs), including those of metal oxides. Water is one of the most precious resources for human life and well-being; however, sources of clean waters become more and more scarce as unsustainable agricultural and industrial practices contribute to ever increasing levels of pollution [1]. A wide range of pollutants, including industrial side-streams, dyes, antibiotics, herbicides and pesticides, are contaminating water resources [2]. Furthermore, microbial contamination leads to serious health problems and even human and animal deaths [3]. The established methods of water purification, including sedimentation [4], flotation [5], filtration [6], adsorption [7], or chlorination [8], are currently in use, but their efficiencies are somewhat limited (e.g., poor efficacy of antibiotics removal) and they associated costs are frequently elevated. The application of NPs for water purification is a novel approach which has significant potential, particularly when nanomaterials with photocatalytic and antimicrobial properties are employed [9]. When exposed to light, such NPs can contribute simultaneously to the organic pollutant removal and elimination of the pathogenic microorganisms. ZnO belongs to the group II–V semiconductor compounds and has a wurtzite crystal structure. ZnO possesses outstanding physical and chemical characteristics, such as a wide direct band gaps (~3.36 eV), high photostability, biocompatibility and low toxicity [10].

Similarly to TiO_2 , ZnO has important photocatalytic properties, induced by ultra-violet (UV) light. When illuminated by light, the ZnO NPs generate reactive oxygen species (ROS) which are crucial for both the antimicrobial and photocatalytic properties of the NPs [11,12]. Therefore, ZnO NPs have significant potential for water treatment applications. Being non-toxic for people and insoluble in water, they can be easily separated and reused. Nevertheless, these characteristics vary with the size, shape and surface area of ZnO NPs. All these characteristics depend on the method of NP synthesis.

Different shapes and sizes of ZnO NPs have been obtained using a number of chemical and physical techniques [13]. Several of these methods are relatively expensive, require controlled pressure and temperature conditions, are energy and time consuming, and frequently employ hazardous chemicals which have negative environmental effects. Triggered by the ever-increasing demand for environmental protection, there is a request for green synthesis methods, which are environmentally benign and avoid employing polluting materials. The biosynthetic approaches, known as “green synthesis”, have recently engaged the interest of scientists worldwide. These approaches have several advantages as compared to traditional physical and/or chemical approaches, such as their easiness, environmentally sustainable nature, moderate costs, and absence of requirements for additional reagents, leading to the production of sustainable green nanoparticles [14]. Green synthesis using plant extracts is the most promising synthesis route among the various biosynthetic approaches currently described. Several types of phytochemicals, such as flavonoids, lignins, alkaloids, tannins and amino acids, are abundantly found in plants. Using distilled water as a universal environmentally friendly solvent, one can conduct green synthesis methods that involve the extraction of water-soluble compounds and apply them as the reductant for the synthesis of metal oxide NPs. Bioactive compounds in the plant extract are a key factor in the formation of nanoparticles using the green synthesis approach. Functional groups of the phytochemicals, such as polyphenols and/or alkaloids, have a capacity to

chelate metal ions, which are then thermally sintered to obtain the NPs of interest. The plant extracts can also play a role of stabilizing agents to prevent the agglomeration of the resulting NPs.

A number of studies focusing on the synthesis and characterization of ZnO nanoparticles using leaf extracts from plants such as *Hibiscus subdariffa* [15], aloe vera [16], *Ficus carica* [17], *Syzygium cumini* [18], *Lupinus albus*, *Lupinus pilosus* [19], and *Sechium edule* [20] have been published within the last decade.

The traditional Brazilian medicinal plant, *Licania tomentosa* Benth (popularly known as Oiti), is a member of the *Chrysobalanaceae* family, an order and superorder of *Rosiflorae rosales*. *Licania* seed oil can be used as a substitute for ink drying oil [21]. Oiti can be encountered within Caatiga bioma, particularly prevalent at the North and Northeast of Brazil. Over 20 genera and about 500 species of trees and shrubs make part of the *Chrysobalanaceae* family, which grow mostly in tropical and subtropical regions [22]. *Licania tomentosa* Benth is widely used as an ornamental tree in Brazilian gardens, roads and squares [23], producing fruits that are ellipticals and drupaceous, which are being collected from December to March [24]. The leaves of *Licania tomentosa* contain betulinic acid; licanolide, a new triterpene lactone; oleanolic acid, lupeol; palmitoleic, hexadecanoic acid [25], phenolics and flavonoids [26] and display antioxidants [26], antibacterials [27] and antiviral activities [28]. The wide availability of Oiti in Brazil and the high quantities of biologically active plant extracts in their leaves caused us to look into their use for ZnO NP synthesis and their applications for photocatalytic degradation of an industrially relevant organic dye.

In our study, for the first time, we synthesize ZnO nanoparticles using the leaf extract of *Licania tomentosa* Benth. The established method is easy to use, inexpensive, and eco-friendly. We used *Licania tomentosa* Benth leaf extract to reduce zinc nitrate hexahydrate $\text{Zn}(\text{NO}_3)_2 \cdot 6\text{H}_2\text{O}$ to ZnO and to promote NP growth. The NPs were characterized using UV–Vis, SEM, XRD, FT-IR and EDS techniques. Moreover, the produced NPs were utilized to photodegrade organic crystal violet (CV) dye. We also compared the efficiency of photodegradation using synthesized ZnO NPs with other metal oxide nanocatalysts.

2. Material and Methods

2.1. Materials

Licania tomentosa leaves have been collected at Sao Carlos USP University campus 2. Zinc nitrate hexahydrate, ethylenediaminetetraacetic acid (EDTA), ascorbic acid (AA) and isopropyl alcohol (IPA) was purchased from Sigma–Aldrich (Sao Paulo, SP, Brazil) and were of analytical quality (purity $\geq 99.0\%$). The chemicals were used as received, without further purification.

2.2. Preparation of the Plant Extract

The *Licania tomentosa* leaves have been collected and thoroughly washed with distilled water to eliminate impurities. The leaves were dehydrated at 50 °C for 5 days and milled into powder. 3.25 g of this powder were mixed with 150 mL of deionized water and vigorously agitated using a magnetic stirrer for 3 h at a room temperature to guarantee an optimized extraction of the soluble bioactive compounds. The mixture, well covered with an aluminum foil, was allowed to rest at room temperature for 21 h and then filtered through Whatman No. 1 paper to remove the residual solids from the clear extract (Figure 1).

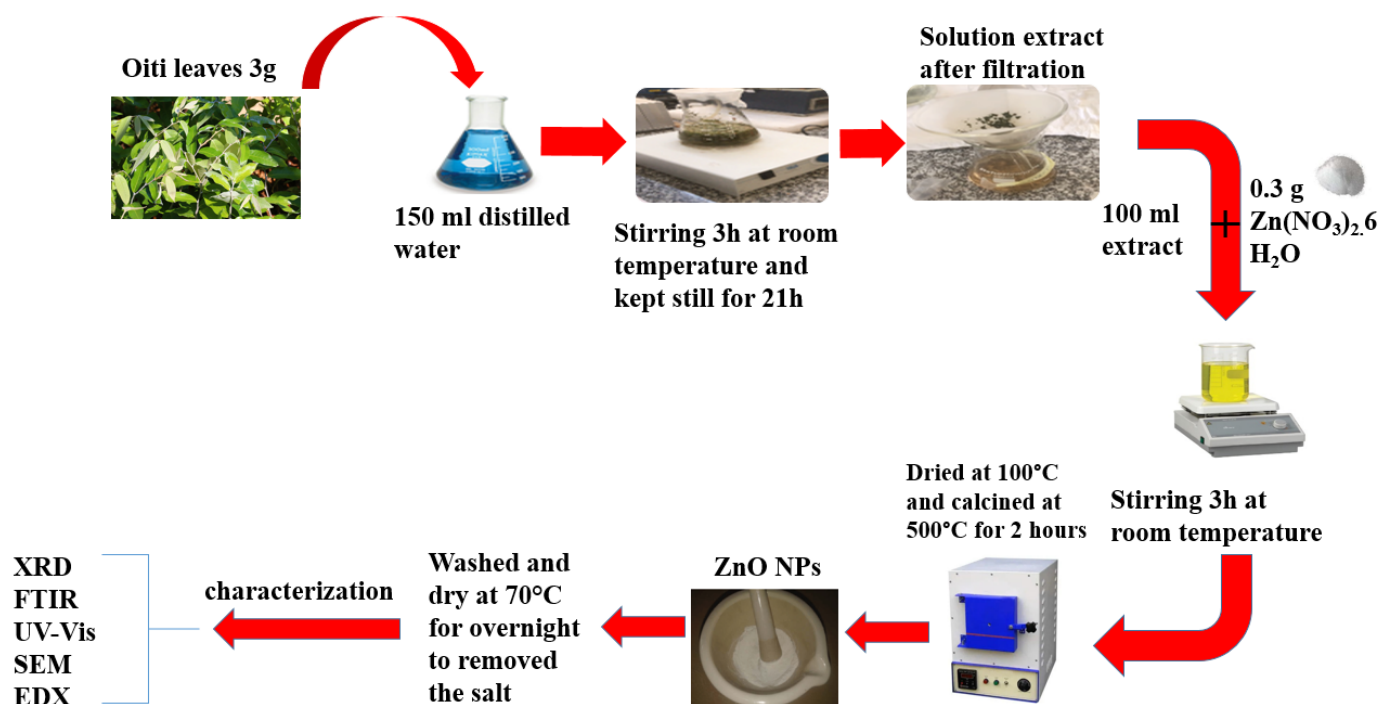


Figure 1. Schematic representation of the green ZnO NPs synthesis using *Licania tomentosa* leaf extract.

2.3. ZnO NPs Synthesis

For ZnO NPs synthesis, 100 mL of the filtered extract were used to dissolve 0.3 g of $\text{Zn}(\text{NO}_3)_2 \cdot 6\text{H}_2\text{O}$ at a room temperature and stirred for 3 h using a magnetic stirrer. The resultant reaction mass was dried in the air oven at 100 °C. A brown-colored paste was obtained and, finally, calcined at 500 °C. White powder was formed, which was then exhaustively washed to remove impurities and dried at 70 °C overnight (Figure 1).

2.4. Physical Characterization of the Obtained Green NPs

The diffraction patterns of the ZnO NPs were obtained using X-ray diffractometer (Bruker Advanced D8) within the angular range of 15–90° with a scan step size of 0.034°. Cu K α radiation was used. The X-ray tube settings were 40 mA and 40 kV. A further analysis of the XRD spectrum was conducted to establish crystal structural parameters such as crystallite size (D), dislocation density (δ), micro-strain (ϵ) and the crystallinity, as described in Equations (1)–(3) [29]:

$$D = \frac{0.9\alpha}{\beta \cos \theta} \quad (1)$$

$$\delta = \frac{1}{D^2} \quad (2)$$

$$\epsilon = \frac{\beta}{4 \tan \theta} \quad (3)$$

Here, D is the average size of the crystallite, α is the wavelength of incident X-rays (1.5406 Å), β is the full-width at half-maximum (FWHM) in radians and θ is the scattering angle in degrees. The lattice constants 'a' and 'c' and the spacing ' d_{hkl} ' for the wurtzite ZnO structure have been calculated according to Equations (2) and (3) [30].

$$a = \sqrt{\frac{1}{3} \frac{\alpha}{\sin \theta}} = \sqrt{\frac{4d_{100}^2}{3}} \text{ and } c = \frac{\alpha}{\sin \theta} = \sqrt{4d_{002}^2} = 2d_{002} \quad (4)$$

$$d_{hkl} = \frac{ac}{2} \sqrt{\frac{3}{c^2(h^2 + hk + K^2) + 3\frac{(al)^2}{4}}} = \frac{\lambda}{2\sin\theta} \quad (5)$$

UV-Vis absorbance spectra were recorded using Thermo Scientific (Waltham, MA, USA) Multiskan GO UV/Vis Microplate Reader Spectrophotometer within the wavelength range 200–1000 nm. The ZnO NPs were suspended in milli-Q water and the absorbance data were collected using 1 cm quartz cuvette. Origin 8 software was used to analyze the absorption spectra.

FT-IR data were collected as follows: pellets of the samples were prepared using a hydraulic press and inserted into a Nicolet 6700 FT-IR spectrometer; the spectra were collected within a wave number range from 400 cm⁻¹ to 4000 cm⁻¹.

The morphology and average size of the prepared NPs were evaluated by the scanning electron microscopy (SEM) technique. The ZnO NP powder was applied on a sample holder and coated with gold. Then, the sample was scanned using a focused electron beam. The elemental composition of the samples was analyzed using energy-dispersive X-ray spectroscopy (EDS) using a X-Max solid-state silicon detector from Oxford Instruments.

2.5. Photocatalytic Activity

The photocatalytic activity of the calcined samples, obtained via the green synthesis of ZnO NPs using *Licania tomentosa* Benth (Oiti) leaf extract, was evaluated using crystal violet (CV) as a model dye. CV is widely used in textile and paper industries and is a component of navy blue and black inks. In a standard photocatalysis experiment, 25 mg of the photocatalyst was dispersed in 100 mL of CV water solution with a dye concentration of 5 mg/L. To achieve adsorption–desorption equilibrium, the mixture was stirred with an absence of light for 60 min. After the dark period, a mixture containing CV and the photocatalyst was irradiated with UV-A light for 120 min using eight (8) UV-A 6W T-5-BL Lucmat lamps (São Paulo, SP, Brazil), each with a power of 6 watts (W) and a maximum wavelength of 368 nanometers (nm). During the course of the experiment, 1.5 mL aliquots were taken every 10 min. The supernatant was obtained by centrifugation at 13,300 rpm for 10 min. The degradation of the pollutant was monitored by measuring the decrease in the maximum absorbance of CV dye in the supernatant, with a peak centered at $\lambda = 583$ nm, using Thermo Scientific Multiskan GO UV/Vis Microplate Reader Spectrophotometer over a wavelength range 200–1000 nm (Figure 2).

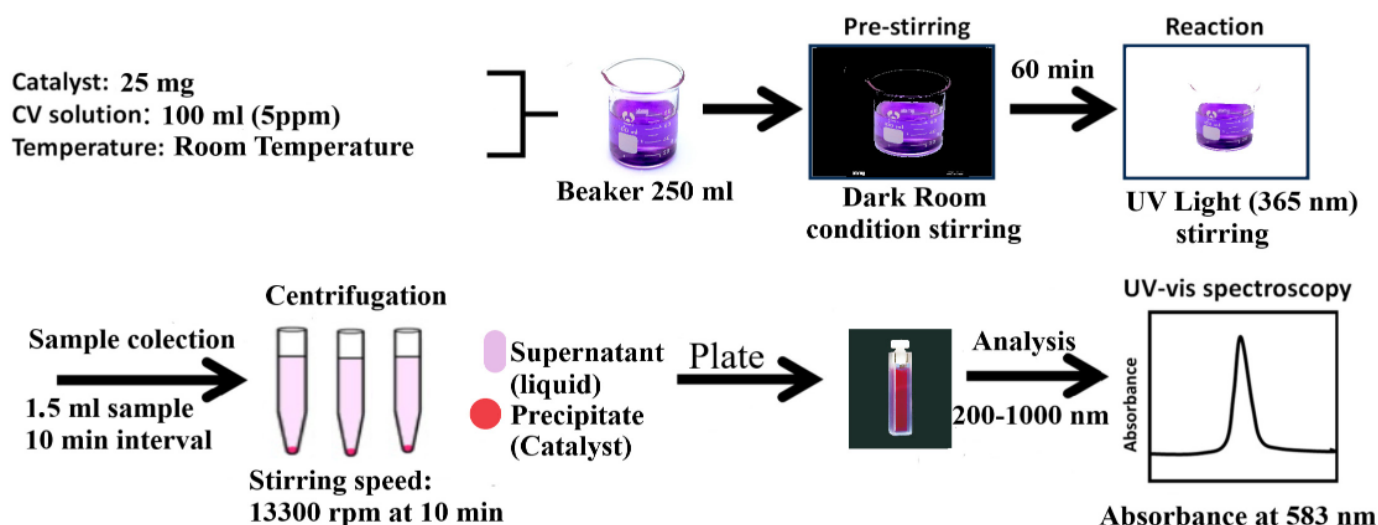


Figure 2. Schematic representation of the experimental steps for CV decomposition.

The degradation was quantified using the equation

$$\text{Degradation percentage} = \frac{C_0 - C_t}{C_0} \times 100 = \frac{A_0 - A_t}{A_0} \times 100 \quad (6)$$

Here, A_0 is the initial absorbance of crystal violet dye corresponding to the initial concentration C_0 , and A_t is the absorbance with concentration C_t at time interval t .

3. Results and Discussion

3.1. Structural Analysis and Average Crystallite Size

The XRD analysis of the green ZnO NPs annealed at 500 °C for 2 h is given in Figure 3. The XRD pattern of the sample (Figure 3) exhibits nine diffraction peaks attributed to the diffraction of X-rays from the (100), (002), (101), (102), (110), (103), (200), (112) and (201) planes. The diffraction peaks were assigned using JCPDS Card No. 36-145, which corresponds to the ZnO wurtzite structure, thermodynamically the most stable phase of ZnO at a room temperature and pressure [31]. All the Bragg peaks were relatively broad, indicating that the NPs indeed were obtained. Using the Debye Scherer formula (Equation (1)), the average crystallite size, dislocation density (δ), and micro-strain (ϵ) of the ZnO NPs was estimated to be about 12.42 nm, $7.1 \times 10^{-3} \text{ nm}^{-2}$ and 0.0081. These results are in good agreement with those reported previously [32]. The summary of the XRD analysis of the biosynthesized ZnO NPs is given in Table 1.

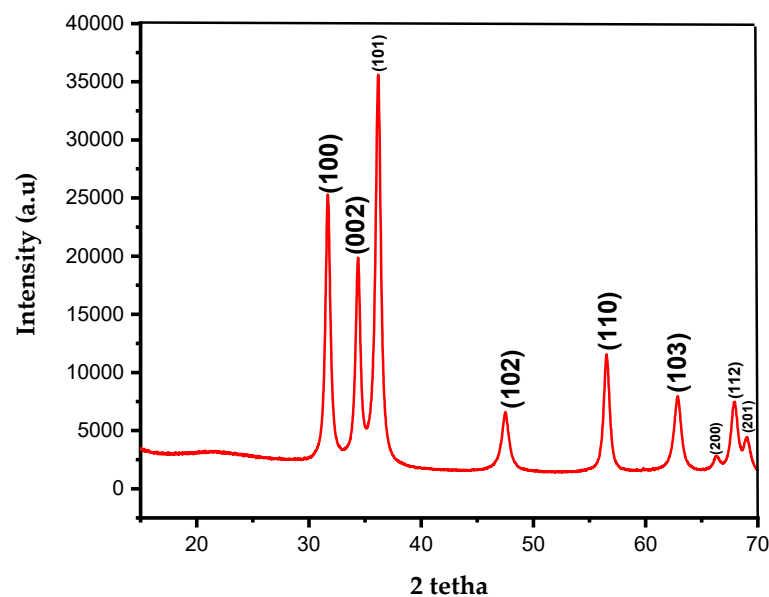


Figure 3. XRD pattern of the ZnO NPs.

Table 1. The X-ray diffraction parameters and crystallite size of the biosynthesized ZnO nanoparticles.

2 Theta Angles (Degree)	(hkl)	Intensities (a.u)	FWHM (Degree)	d(hkl), nm	Crystallite Size (nm)
31.68	(100)	13,937.40	0.64358	0.28221086	11.88
34.39	(002)	10,991.96	0.72921	0.26056687	10.41
36.19	(101)	20,470.9	0.6853	0.24800907	11.02
47.51	(102)	1953.19	0.56568	0.19122373	12.85
56.53	(110)	4242.09	0.55264	0.16266489	12.66

Table 1. Cont.

2 Theta Angles (Degree)	(hkl)	Intensities (a.u)	FWHM (Degree)	d(hkl), nm	Crystallite Size (nm)
62.88	(103)	2599.33	0.60442	0.14767869	11.21
66.32	(200)	2879.18	0.46	0.1408281	14.46
67.94	(112)	2353.67	0.6019	0.13785914	10.95
69.01	(201)	4099.63	0.4	0.13598053	16.37
Mean crystallite size, nm					12.4
dislocation density (δ), nm ⁻²					0.0071
Micro-strain (ϵ)					0.0081

3.2. SEM Analysis

The SEM technique was applied to analyze morphology and to estimate the particle size of the green ZnO NPs (Figure 4a). The biosynthesized ZnO NPs have a homogeneously spherical morphology and are assembled in the aggregates (Figure 4a). In Figure 4b, the histogram of particle size distribution shows that the mean diameter of ZnO nanoparticles is 35.68 nm. A comparison of the average ZnO NP size (Figure 4b) with the mean size of the crystallites (Table 1) indicates that the synthesized particles are polycrystalline. To analyze the chemical composition of the biosynthesized sample, energy-dispersive X-ray spectra (EDS) were collected, as depicted in Figure 4c. The EDS spectrum reveals the presence of three main elements (zinc, oxygen and silicon) in the prepared ZnO NPs. The silicon signal originates from the Si grids used for the sample loading.

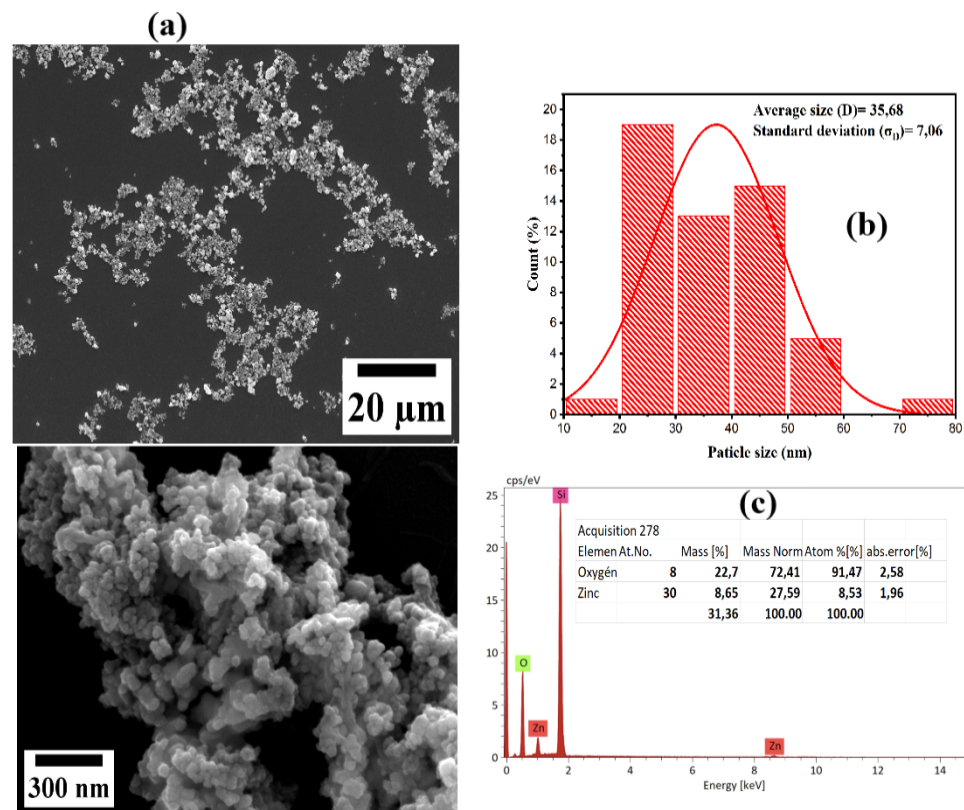


Figure 4. (a) ZnO NPs, as observed by SEM; (b) distribution of particle sizes; (c) EDS of ZnO nanoparticles.

3.3. UV-Vis Spectroscopy

UV-Vis absorption spectroscopy was applied to analyze the optical properties of the green ZnO NPs. Figure 5 shows the UV-Vis ZnO NPs absorption spectrum from 200 to 1000 nm. The figure shows a clear absorption peak at 354 nm that illustrates the presence of ZnO NPs. The band gap energy of the ZnO NPs was estimated from the experimental UV-Vis spectroscopy based on Equation (5) [33].

$$(\alpha h\nu)^2 = B(h\nu - E_g)^{1/2} \quad (7)$$

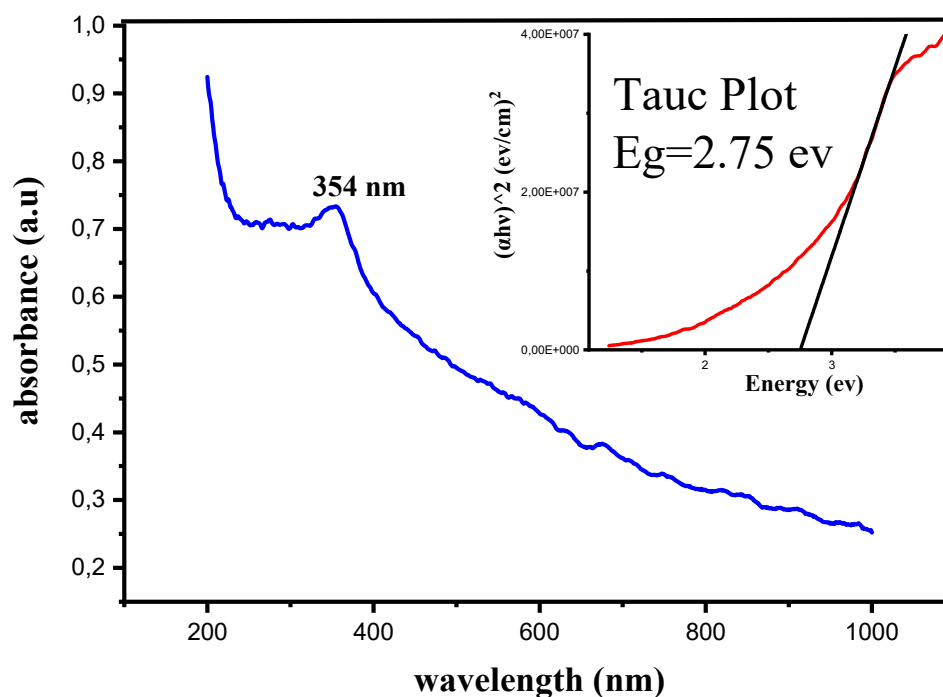


Figure 5. UV-Vis spectrum of ZnO nanoparticles prepared by *Licania tomentosa* leaf extract, inset: Tauc plot of the same UV-Vis spectrum.

Here, B is a constant, h is the Planck constant ($6.626 \times 10^{-34} \text{ J Hz}^{-1}$), ν is the light frequency, E_g is the optical band gap energy and α is the absorption coefficient.

The specific band gap was determined using the extrapolation of the linear part of the $(\alpha h\nu)^2$ versus $(h\nu)$ function to the x -axis. The band gap of the ZnO NPs was determined as 2.75 eV (see insert in Figure 5). This gap is significantly smaller than expected for bulk ZnO ($E_g = 3.37 \text{ eV}$) [34]. A decrease in the band gap is expected as a consequence of tiny NP dimensions and also as a result of the plant extract reduction [35], which can lead to even more reactive NPs than the equivalent NPs prepared using other procedures [36,37].

3.4. FT-IR Spectroscopy Analysis

The FT-IR spectra of ZnO nanoparticles measured in the range of 400–4000 cm^{-1} showed various shifts and differences in the peak areas at 3400 cm^{-1} , 1550 cm^{-1} , 1400 cm^{-1} , 1050 cm^{-1} and 550 cm^{-1} (Figure 6). The peak near 550 cm^{-1} corresponded to the Zn–O bond, which further supported the notion of ZnO nanoparticle synthesis [30]. An intense peak at 3400 cm^{-1} could be attributed to the O–H stretching vibrations, originating from the chemically bound OH group and/or the moisture adsorbed on the ZnO nanoparticle surface, whereas a less intense peak at 1550 cm^{-1} arises from the deformation vibrations of the same groups [38,39]. Similarly, the peaks that appeared at 1400 cm^{-1} and 1050 cm^{-1} can be associated with the C–O stretching modes [40,41].

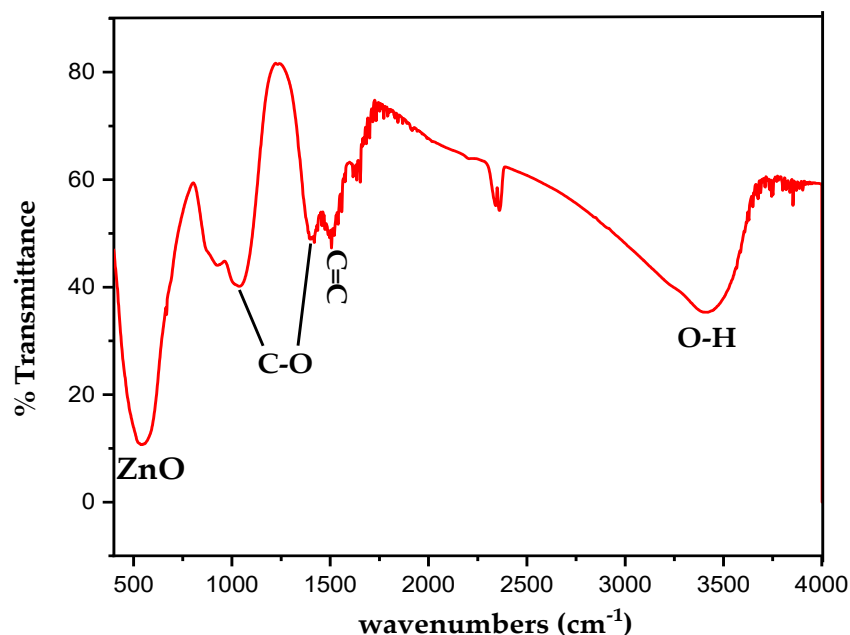


Figure 6. FT-IR spectrum of ZnO nanoparticles synthesized using *Licania tomentosa* leaf extract. Main FT-IR peaks are labeled.

3.5. Photocatalysts Activity

The photocatalytic degradation profile of crystal violet dye by the ZnO NPs illuminated with light is shown in Figure 7a. After 120 min of UV-light exposure, ~79% of the CV dye were photodegraded, demonstrating the excellent photodegradation potential of the prepared ZnO NPs. The degradation rate can be computed by calculating the ratio of CV dye concentration in the course of exposure to light to the initial concentration $[\ln(C/C_0)]$ versus the illumination time t (Figure 7c). The dependance of $\ln(C/C_0)$ and t for the ZnO NPs sample is linear and the correlation coefficient $R^2 = 0.99$ is high (Figure 7c), indicating that the catalytic mechanism proceeds via the first-order kinetic model described by the following equation [31]:

$$\ln \frac{C}{C_0} = k t \quad (8)$$

where k is the apparent reaction rate constant. The value of k is proportional to the concentration of catalytic sites responsible for degradation.

The half-life time ($t_{1/2}$) required to reduce the dye concentration by half is computed as follows:

$$t_{1/2} = \frac{\ln 2}{k} \quad (9)$$

k is obtained from the slope of the line in Figure 7c [17]. The calculated value of k and $t_{1/2}$ are 0.0102 min^{-1} and ~70 min, respectively.

The high reaction rate constant and short half-life time of CV degradation by the ZnO NPs is consistent with highly efficient degradation of the dye.

The performance of various ZnO photocatalysts for CV dye degradation under UV light is given in Table 2. The high efficiency of photocatalytic degradation of the green ZnO NPs obtained in this study might be related to the larger active surface area of the photocatalyst as compared to the similar ZnO NPs obtained by different methods (Table 2).

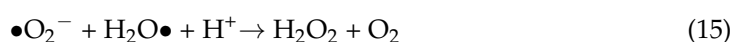
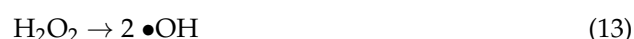
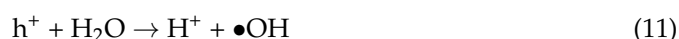
Table 2. Cont.

Chemical Synthesis						
Catalyst Load (mg)	Light Source	Removal Efficiency (%)	Initial Dye Concentration (ppm)	Rate Constant K (min^{-1})	Synthesis Method	Ref.
50	UV Not reported	98 (90 min)	10	not reported	Leucocephala leaf extract	[46]
20	UV (500 W)	86 (90 min)	10	0.00624	Delonix Elata Leaf extract	[47]
25	UV (48 W)	79 (120 min)	5	0.0102	Oiti leaf extract	This work

On the other hand, rod-like $\alpha\text{-MnO}_2$ nanocatalysts at a concentration of 30 mg/L were shown to degrade a wide range of cationic and anionic dyes (Rhodamine B, Rhodamine-6G, Congo Red, Methyl Blue and Methyl Orange) with very high efficiencies of between 95 and 99.9% within 10 min using visible incident light with an intensity of 8 mW/cm² and a spectral range within 400–600 nm with a central wavelength of 445 nm [48]. At the same time, much smaller degradation rates (30 to 50%) of MB dye have been reported for CeO₂ and MnO₂ nanoparticles in [49], supporting the notion that the synthetic procedures and resulting chemical and physical properties of the obtained NPs have a strong impact on their photocatalytic performance.

3.6. Mechanism of CV Dye Degradation

The mechanism of CV dye photodegradation is shown in the reactions (10)–(16) [44]. The water splitting reaction starts with the UV photoexcitation of the ZnO electrons. The resulting electron hole of the ZnO NP works as an active site [50]. The ionization of a water molecule happens when the water interacts with the electron hole and is being ionized into a proton (H^+) and a radical $\bullet\text{OH}$. The formation of the $\bullet\text{OH}$, being a strong oxidizing agent, is crucial for dye decomposition. Simultaneously, superoxide ($\bullet\text{O}_2^-$) is formed when an oxygen molecule interacts with the electron from the catalyst. The $\bullet\text{O}_2^-$ can be protonated to form a hydroperoxyl radical ($\text{HOO}\bullet$), which might be further transformed into $\bullet\text{OH}$. Consequently, the chemical decomposition of the dye is a result of its interaction with $\bullet\text{OH}$. Moreover, the dye can also interact with the electron hole in the valence band and the electron in the conduction band to form oxidation and reduction products [50].



To experimentally investigate the role of particular ROS, we supplemented the photodegradation process with isopropyl alcohol (IPA, 10 mM), ascorbic acid (AA, 10 mM) or ethylenediaminetetraacetic acid (EDTA, 2 mM), which are the chemical scavengers

for $\bullet\text{OH}$, $\bullet\text{O}^{2-}$ and H^+ , respectively. The impacts of the scavengers on the efficiency of photocatalytic degradation can be seen in Figure 7d. The strongest suppression of the photocatalytic reaction was observed for AA, revealing that superoxide $\bullet\text{O}^{2-}$ plays a leading role in the CV photodegradation. IPA and EDTA also had negative effects on the rate of the photocatalytic degradation of CV, but their impact was less severe. This indicates that H^+ and $\bullet\text{OH}$ also play important roles but are somewhat less important than superoxide ions in the photocatalytic reaction.

Thus, we can conclude that effective photoexcitation, leading to an efficient water spitting reaction and reactive oxygen species generation, is central to CV dye decomposition. The small bandgap of the synthesized ZnO NPs combined with the appropriate light source resulted in the observed high efficiency of the dye degradation (Table 2). The final products of the photocatalytic reaction are typically less harmful or more easily removable than the original dye (Figure 8) [44].

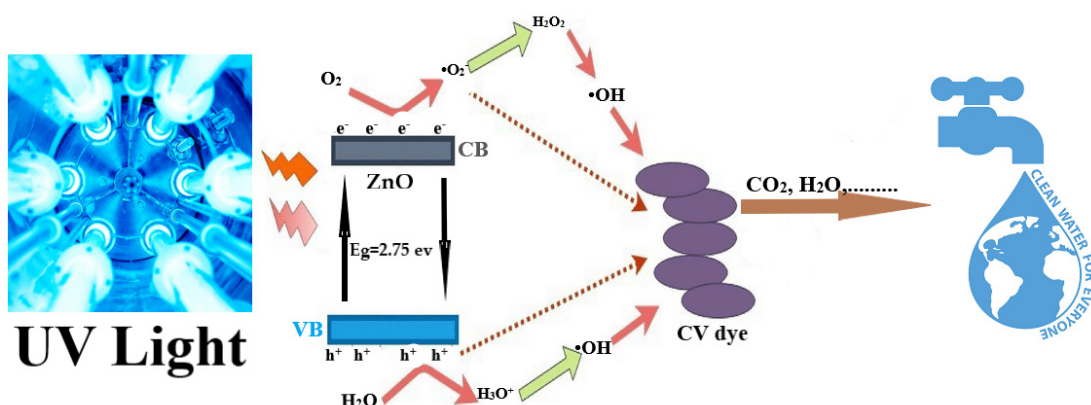


Figure 8. Scheme of the photocatalytic degradation routes.

3.7. Optimization Studies

The prepared ZnO NPs were subjected to further optimization in order to establish the optimum catalyst loading and temperature, the intensity of the irradiation source and the pH.

3.7.1. Optimization of ZnO Catalyst Loading

In general, an increase in the photocatalyst load in the photocatalytic assay would lead to an increased production of $\bullet\text{OH}$ free radicals. In this study, the oxidative degradation of CV was conducted by studying the catalyst loadings of 12.5, 25 and 50 mg while keeping constant CV dye concentration (5 ppm) (Figure 9). After 120 min of UV exposure, the degradation of the dye increased from 36% to 79%, when the ZnO NPs loading increased from 12.5 mg to 25 mg. An increase in the catalyst loading amplifies a number of the available active sites, resulting in an increased efficiency of photocatalytic degradation as a result of the higher NP density in the illuminated area [49]. However, upon a further increase in the catalyst loading to 50 mg, the degradation efficiency of the dye was found to be reduced to 74%. This might be attributed to the enhanced light scattering and screening effects due to the increase in the catalyst NPs load, thus limiting the catalytic performance of ZnO NPs [51,52]. In addition, catalyst aggregation is detrimental to its catalytic activity [46]. Thus, the optimal amount of ZnO NPs for optimal degradation efficiency under the conditions of the current study was found to be 25 mg.

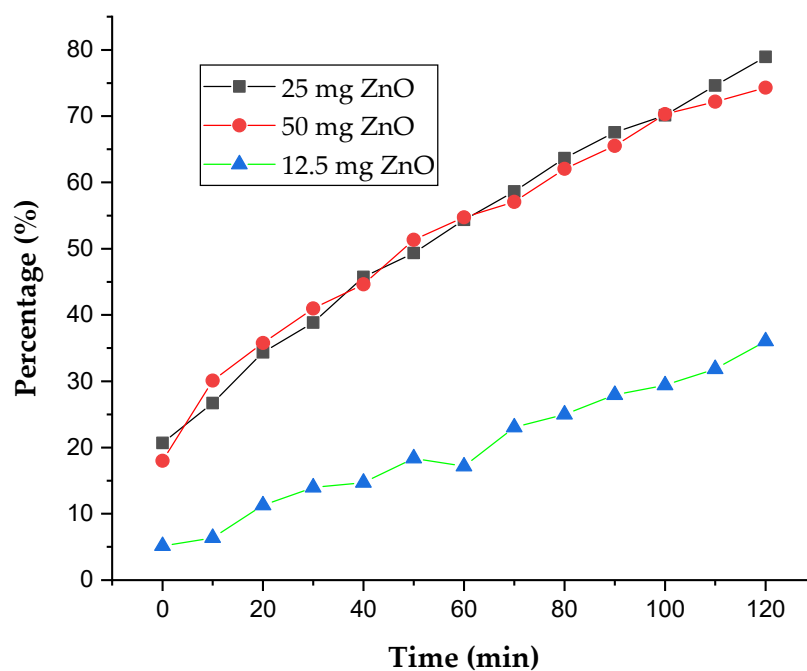


Figure 9. Impact of the catalyst loading on the performance of ZnO NPs photocatalyst against CV.

3.7.2. Effect of Temperature

Normally, ambient conditions are employed for monitoring the light-mediated NP degradation reactions, as applied for the degradation of dyes. However, temperature can influence the kinetics of the degradation processes [51]. We evaluated CV dye photodegradation by a ZnO NP catalyst at three distinct reaction temperatures: 40, 50 and 60 °C (Figure 10). After a 120 min reaction at these temperatures, the CV decolorization efficiencies were almost the same, such that the efficiency of decolorization varied between 75%, 77% and 78%, as compared to 79% at room temperature, revealing that the heterogeneous catalytic photodegradation was not significantly affected by temperature [53].

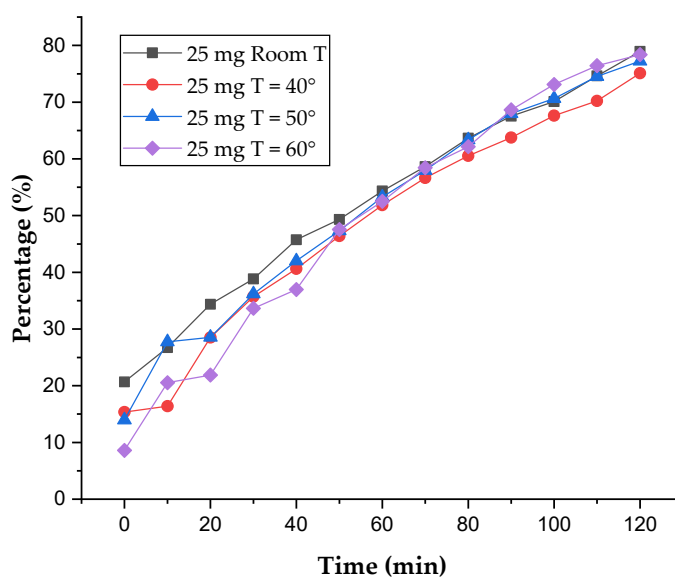


Figure 10. Influence of the reaction temperature on the photocatalytic degradation of CV dye.

3.7.3. Impact of UV Light Intensity

To investigate the influence of UV light intensity levels on the photodegradation of CV, as promoted by the ZnO NPs, the UV lamps with a total power of 24 W and 48 W

were employed while the initial CV concentration and catalyst loading were set to 5 ppm and 25 mg, respectively. The experiments were conducted both in the presence of light and in the dark (Figure 11). Our results show that the efficiency of photodegradation is strongly impacted by the light intensity. Indeed, with an increase in UV light intensity from 24 W to 48 W, the level of CV degradation increases from 50% to 79%. Since the ZnO NPs are suspended in a stirred solution, the light intensity directly affects a number of photons which hit the catalyst surface. The increase in degradation rates and efficiencies is due to the increased generation of ROS on the ZnO NP surface under a more intense light condition. As expected, at the absence of light, the ZnO catalyst was unable to promote the efficient oxidation of the dye (Figure 11) [54,55].

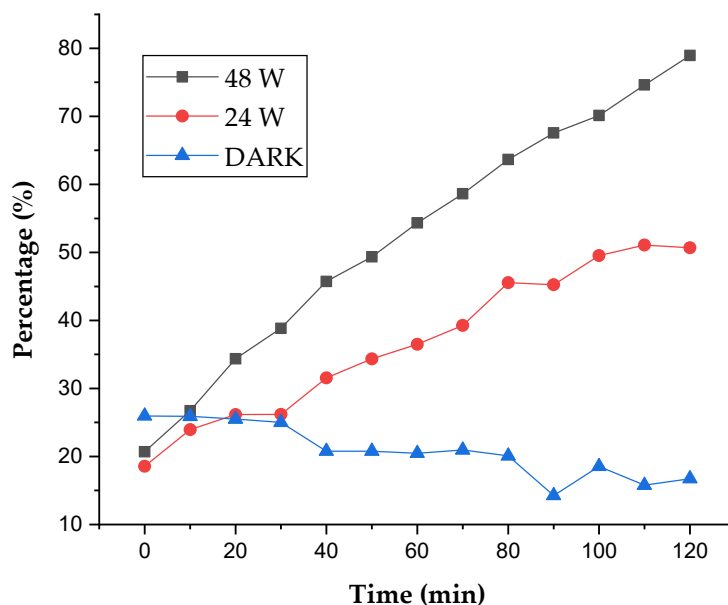


Figure 11. Impact of light intensity on photocatalytic degradation of CV dye.

3.7.4. Effect of pH

The pH influence on the efficiency of dye degradation was studied by varying the solution pH in the range of 6–8 while holding the catalyst dosage and initial dye concentration at the fixed values of 25 mg and 5 ppm, respectively. The pH of the solution was adjusted using hydrochloric acid (HCl) and sodium hydroxide (NaOH) solutions. The results of pH dependency studies are depicted in Figure 12. These experiments reveal that a stronger dye degradation was observed for a relatively high pH of 8.85, as compared to acid (pH = 6.65) conditions. Indeed, it is well documented that the pH of zero-point charge (pH_{zpc}) for ZnO NPs is alkaline (between 8.0 and 9.0) [54,56], which means that it is positive at acid pHs (pH = 6) and is close to neutral or negatively charged at alkaline pHs (pH ≥ 8).

The first-order rate constants of all the parameters estimated from $\ln C_0/C$ vs. time plot are given in Table 3.

Table 3. The effect of key parameters on the rate of degradation of crystal violet by the ZnO NPs under UV-A light for a maximum duration of 120 min.

Parameters	K (min ^{−1})	T _{1/2} (min)	R ²
Catalyst loading (mg)			
25	0.0102	67.95	0.99486
50	0.00927	74.77	0.99474
12.5	0.00328	211.32	0.97806

Table 3. Cont.

Parameters	K (min ^{−1})	T _{1/2} (min)	R ²
Temperature (degree)			
Room	0.0102	67.95	0.99486
40	0.00911	76.08	0.99039
50	0.01099	63.07	0.99327
60	0.0122	56.81	0.9725
UV intensity (watt)			
36	0.00465	149.06	0.98055
72	0.0102	67.95	0.99486
pH			
6.65	0.0036	192.54	0.97801
8.85	0.0102	67.95	0.99486

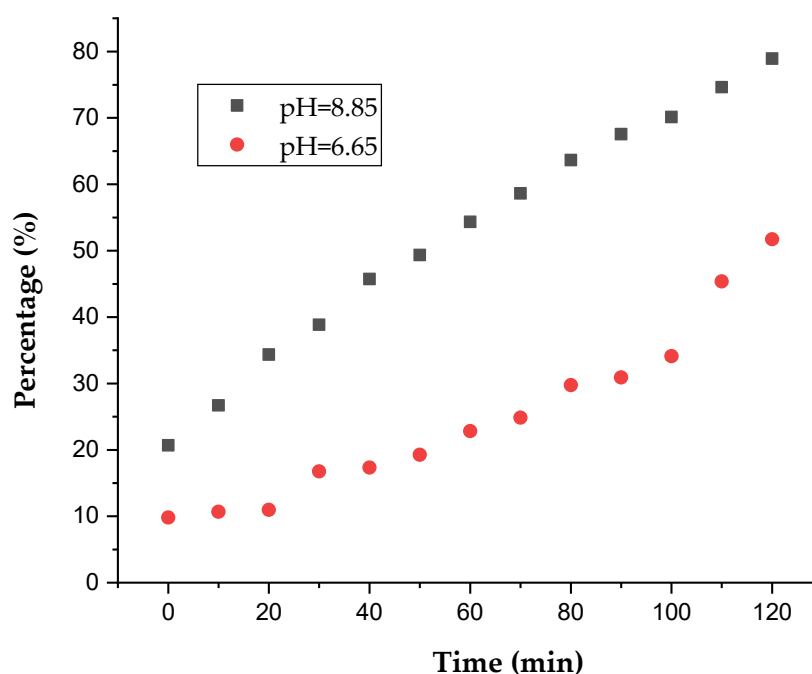


Figure 12. Effect of pH on photocatalytic degradation of CV dye.

To investigate the impact of the photocatalytic process on the photocatalyst itself, we recovered the ZnO NPs at the end of the cycle and subjected them to an XRD analysis. The XRD studies reveal a well-preserved crystalline structure (Figure 13).

The crystallinity, the dislocation constant, the microstrain and the average size of the ZnO nanoparticles biosynthesis before and after the photocatalytic degradation were calculated from the XRD patterns and summarized in Table 4.

Our results demonstrate that UV light illumination of the ZnO NPs leads to an increase in the average crystallite size and a decrease in the dislocation density (Table 4), indicating a possible annealing effect. At the same time, the crystallinity of the nanocatalyst decreases, which is related to its increased amorphization. In addition, specific surface area, the nature and concentration of electronic defects, as well as surface contaminants were shown to have strong impacts on the nanocatalyst photocatalytic performances [57].

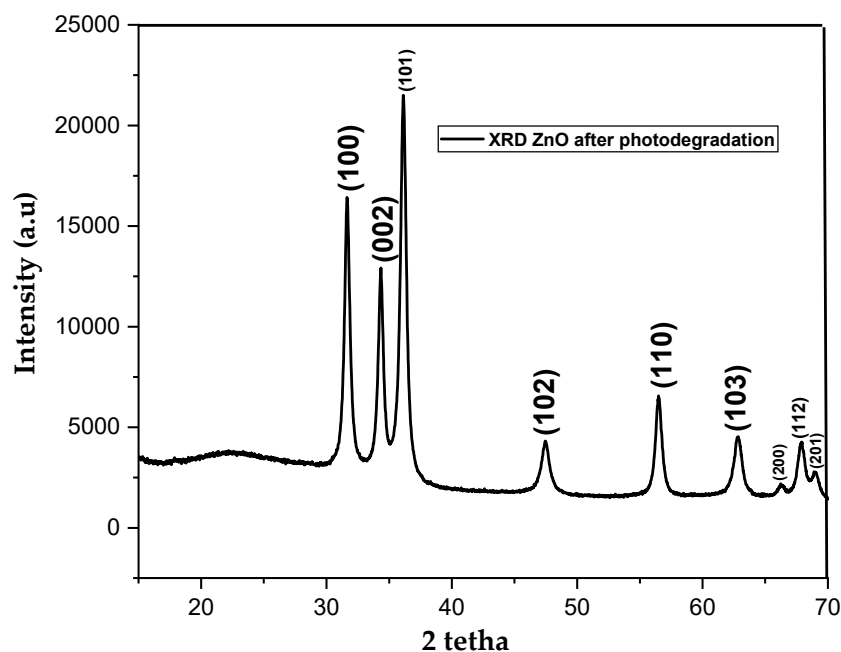


Figure 13. XRD of ZnO NPs after photodegradation of CV dye.

Table 4. Crystallinity, dislocation constant, microstrain and average crystallite size for the bioengineered ZnO nanoparticles after the photocatalytic degradation.

	Average Crystallite Size (nm)	Dislocation Density (δ) (nm^{-2})	Microstrain (ϵ)	Crystallinity (%)
Before	12.4	0.0071	0.0081	50.83
After	13.32	0.0056	0.0072	32.67

4. Conclusions

The total use of plant biomass is crucial for the building of a circular bioeconomy. Aiming to valorize an underappreciated part of plant biomass, extractives, a sustainable synthesis of ZnO NPs using *Licania tomentosa* Benth (also known as Oiti) leaf extract has been performed for the first time and the NP properties have been evaluated. The produced bioengineered ZnO NPs were characterized using a range of physical techniques. We further applied the ZnO NPs for the photocatalytic degradation of crystal violet (CV) dye and evaluated the efficiency of the photodegradation process. The synthesized nanoparticles have a mean crystallite size of 12.4 nm, as measured by XRD, and have a spherical shape, as revealed by SEM. UV–Vis studies show that ZnO NPs have a direct band gap of 2.72 eV, as estimated by a Tauc plot. The photodegradation activity tests using synthesized green ZnO NPs revealed that up to ~79% of CV dye could be decomposed under UV irradiation in 2 h under experimentally studied conditions. We also demonstrated that the decomposition of CV is directly influenced by the catalyst load and the light source intensity and that the nanocatalyst largely preserves its structural properties after the photodegradation cycle.

Author Contributions: M.T., A.d.J.B., V.d.O.A.P. and I.P. designed the experiments; M.T. and A.d.J.B. synthesized the NPs, M.T., A.d.J.B., J.F.P., V.S.V. and T.S.M. conducted characterization of the NPs; B.D.N., Z.W.D., S.V. and V.S.V. contributed with scientific discussions and further characterization of the NPs; M.T. and J.F.P. conducted photodegradation studies; M.T., V.d.O.A.P. and I.P. wrote the manuscript with the input from all the other authors; I.P., V.S.V., F.T.T., B.Q.M. and B.B.M. secured funding, and I.P. and V.S.V. supervised the project. All authors have read and agreed to the published version of the manuscript.

Funding: This work was supported by the Fundação de Amparo à Pesquisa do Estado de São Paulo (FAPESP, grants #2021/08780-1 and 2024/00533-3 to I.P.) and by the Conselho Nacional de Desenvolvimento Científico e Tecnológico (CNPq, grants #306852/2021-7 and 440180/2022-8 to I.P.) and by CAPES to M.T. Partial support provided by the BRICS-NRF project Grant no. 150501, Unrated NRF grant Reference/Grant Number: SRUG2204305453 and DRSP grant from UNISA are acknowledged. Z.W.D. wants to acknowledge the CUT-UFS Seed grant for the MIT project and the NRF Africa University Twinning project (grant number AUTP240325210690).

Data Availability Statement: The original contributions presented in this study are included in the article. Further inquiries can be directed to the corresponding author.

Acknowledgments: We acknowledge support of multiuser facilities of IFSC and IQSC/USP to allow for SEM and EDS measurements.

Conflicts of Interest: The author declares no conflicts of interest.

References

1. Zolkefli, N.; Sharuddin, S.S.; Yusoff, M.Z.M.; Hassan, M.A.; Maeda, T.; Ramli, N. A review of current and emerging approaches for water pollution monitoring. *Water* **2020**, *12*, 3417. [\[CrossRef\]](#)
2. Arman, N.Z.; Salmiati, S.; Aris, A.; Salim, M.R.; Nazifa, T.H.; Muhamad, M.S.; Marpongahtun, M. A review on emerging pollutants in the water environment: Existences, health effects and treatment processes. *Water* **2021**, *13*, 3258. [\[CrossRef\]](#)
3. Ferreira, V.; Magalhães, R.; Teixeira, P.; Castro, P.M.L.; Calheiros, C.S.C. Occurrence of fecal bacteria and zoonotic pathogens in different water bodies: Supporting water quality management. *Water* **2022**, *14*, 780. [\[CrossRef\]](#)
4. Castro-Jiménez, C.C.; Saldarriaga-Molina, J.C.; García, E.F.; Correa-Ochoa, M.A. Primary treatment of domestic wastewater with the use of unmodified and chemically modified drinking water treatment sludge. *Sustainability* **2022**, *14*, 9827. [\[CrossRef\]](#)
5. Constantin, C.; Popescu, I.C.; Oprea, O.; Stoica, L. U (VI) removal from diluted aqueous systems by sorption–flotation. *Sci. Rep.* **2022**, *12*, 16951. [\[CrossRef\]](#) [\[PubMed\]](#)
6. Nechifor, A.C.; Cotorcea, S.; Bungău, C.; Albu, P.C.; Pașcu, D.; Oprea, O.; Grosu, A.R.; Pîrțac, A.; Nechifor, G. Removing of the sulfur compounds by impregnated polypropylene fibers with silver nanoparticles-cellulose derivatives for air odor correction. *Membranes* **2021**, *11*, 256. [\[CrossRef\]](#)
7. Petrișor, G.; Motelica, L.; Fica, D.; Ilie, C.-I.; Trușcă, R.D.; Surdu, V.-A.; Oprea, O.-C.; Mîrț, A.-L.; Vasilievici, G.; Semenescu, A.; et al. Increasing bioavailability of trans-ferulic acid by encapsulation in functionalized mesoporous silica. *Pharmaceutics* **2023**, *15*, 660. [\[CrossRef\]](#)
8. Adefisoye, M.A.; Olaniran, A.O. Does chlorination promote antimicrobial resistance in waterborne pathogens? Mechanistic insight into co-resistance and its implication for public health. *Antibiotics* **2022**, *11*, 564. [\[CrossRef\]](#)
9. Spoială, A.; Ilie, C.-I.; Dolet, G.; Croitoru, A.-M.; Surdu, V.-A.; Trușcă, R.-D.; Motelica, L.; Oprea, O.-C.; Fica, D.; Fica, A.; et al. Preparation and characterization of chitosan/TiO₂ composite membranes as adsorbent materials for water purification. *Membranes* **2022**, *12*, 804. [\[CrossRef\]](#)
10. Sudiarti, T.; Ulpah, F.; Sanusi, Listiani, P.; Ichikawa, Y.; Honda, M.; Amelia, S.R.; 'Adany, F.; Nurrosyid, N.; Ivansyah, A.L. Unlocking the photocatalytic and antibacterial properties of triple and quadruple doped ZnO nanoparticles (Mg/Cu/N-ZnO and Mg/Cu/N/B-ZnO) prepared by one pot facile solid state synthesis. *Adv. Powder Technol.* **2024**, *35*, 104567. [\[CrossRef\]](#)
11. Khan, A.K.; Renouard, S.; Drouet, S.; Blondeau, J.-P.; Anjum, I.; Hano, C.; Abbasi, B.H.; Anjum, S. Effect of UV irradiation (A and C) on *Casuarina equisetifolia*-mediated biosynthesis and characterization of antimicrobial and anticancer activity of biocompatible zinc oxide nanoparticles. *Pharmaceutics* **2021**, *13*, 1977. [\[CrossRef\]](#) [\[PubMed\]](#)
12. Joseph, J.A.; Nair, S.B.; John, S.S.; Remillard, S.K.; Shaji, S.; Philip, R.R. Zinc-doped iron oxide nanostructures for enhanced photocatalytic and antimicrobial applications. *J. Appl. Electrochem.* **2021**, *51*, 521–538. [\[CrossRef\]](#)
13. Ikhtayies, S.J. Synthesis of ZnO microrods by the spray pyrolysis technique. *J. Electron. Mater.* **2016**, *45*, 3964–3996. [\[CrossRef\]](#)
14. Singh, J.; Dutta, T.; Kim, K.H.; Rawat, M.; Samddar, P.; Kumar, P. 'Green' synthesis of metals and their oxide nanoparticles: Applications for environmental remediation. *J. Nanobiotechnology* **2018**, *16*, 84. [\[CrossRef\]](#)
15. Bala, N.; Saha, S.; Chakraborty, M.; Maiti, M.; Das, S.; Basu, R.; Nandy, P. Green synthesis of zinc oxide nanoparticles using Hibiscus subdariffa leaf extract: Effect of temperature on synthesis, anti-bacterial activity and anti-diabetic activity. *RSC Adv.* **2015**, *5*, 4993–5003. [\[CrossRef\]](#)
16. Sharma, S.; Kumar, K.; Thakur, N.; Chauhan, S.; Chauhan, M.S. The effect of shape and size of ZnO nanoparticles on their antimicrobial and photocatalytic activities: A green approach. *Bull. Mater. Sci.* **2020**, *43*, 20. [\[CrossRef\]](#)

17. Arumugam, J.; Thambidurai, S.; Suresh, S.; Selvapandiyan, M.; Kandasamy, M.; Pugazhenthiran, N.; Kumar, S.K.; Muneeswaran, T.; Quero, F. Green synthesis of zinc oxide nanoparticles using *Ficus carica* leaf extract and their bactericidal and photocatalytic performance evaluation. *Chem. Phys. Lett.* **2021**, *783*, 139040. [\[CrossRef\]](#)
18. Sadiq, H.; Sher, F.; Sehar, S.; Lima, E.C.; Zhang, S.; Iqbal, H.M.; Zafar, F.; Nuhanović, M. Green synthesis of ZnO nanoparticles from *Syzygium cumini* leaves extract with robust photocatalysis applications. *J. Mol. Liq.* **2021**, *335*, 116567. [\[CrossRef\]](#)
19. Mirza, S.; Hussaini, A.A.; Öztürk, G.; Turgut, M.; Öztürk, T.; Tugay, O.; Ulukuş, D.; Yıldırım, M. Photocatalytic and antibacterial activities of ZnO nanoparticles synthesized from *Lupinus albus* and *Lupinus pilosus* plant extracts via green synthesis approach. *Inorg. Chem. Commun.* **2023**, *155*, 111124. [\[CrossRef\]](#)
20. Elavarasan, N.; Kokila, K.; Inbasekar, G.; Sujatha, V. Evaluation of photocatalytic activity, antibacterial and cytotoxic effects of green synthesized ZnO nanoparticles by *Sechium edule* leaf extract. *Res. Chem. Intermed.* **2017**, *43*, 3361–3376. [\[CrossRef\]](#)
21. Andrade, E.H.A.; Zoghbi, M.G.B.; Maia, J.G.S. Constituintes volateis dos frutos de *Licania tomentosa*. *Acta Amaz.* **1998**, *28*, 55–58. [\[CrossRef\]](#)
22. Carnevale Neto, F.; Pilon, A.C.; da Silva Bolzani, V.; Castro-Gamboa, I. Chrysobalanaceae: Secondary metabolites, ethnopharmacology and pharmacological potential. *Phytochem. Rev.* **2013**, *12*, 121–146. [\[CrossRef\]](#)
23. Zamproni, K.; Biondi, D.; Maria, T.R.B.C.; Louveira, F.A. Diagnóstico quali-quantitativo da arborização viária de Bonito, Mato Grosso do Sul. *Floresta* **2018**, *48*, 235–244. [\[CrossRef\]](#)
24. Monteiro, K.L.; de Oliveira, C.; da Silva, B.M.; Moro, F.V.; de Carvalho, D.A. Morphological characteristics of fruit, seed and post-seminal development of *Licania tomentosa* (Benth.) Fritsch/Caracterizacão morfológica de frutos, de sementes e do desenvolvimento pos-seminal de *Licania tomentosa* (Benth.) Fritsch. *Cienc. Rural* **2012**, *42*, 90–98. [\[CrossRef\]](#)
25. Castilho, R.O.; Kaplan, M.A.C. Chemical constituents of *Licania tomentosa* Benth. (Chrysobalanaceae). *New Chem.* **2008**, *31*, 66–69.
26. Macêdo, J.B.M. Capacidade Antioxidante In Vitro e Avaliação da Toxicidade Aguda In Vivo de Extratos de Folhas de *Licania rígida* Benth., *Licania tomentosa* (Benth.) Fritsch e *Couepia* Imprensa France (Chrysobalanaceae). Master's Thesis, Universidade Federal do Rio Grande do Norte, Natal, Brazil, 2011.
27. Farias, D.F.; Souza, T.M.; Viana, M.P.; Soares, B.M.; Cunha, A.P.; Vasconcelos, I.M.; Ricardo, N.M.P.S.; Ferreira, P.M.P.; Melo, V.M.M.; Carvalho, A.F.U. Antibacterial, antioxidant, and anticholinesterase activities of plant seed extracts from Brazilian semiarid region. *BioMed Res. Int.* **2013**, *2013*, 510736. [\[CrossRef\]](#)
28. Agra, M.D.F.; De Freitas, P.F.; Barbosa-filho, J.M. Divulgação Synopsis of the plants known as medicinal and poisonous in Northeast of Brazil. *Rev. Bras. Farmacogn.* **2007**, *17*, 114–140. [\[CrossRef\]](#)
29. Prakoso, S.P.; Saleh, R. Synthesis and spectroscopic characterization of undoped nanocrystalline ZnO particles prepared by co-precipitation. *Mater. Sci. Appl.* **2012**, *3*, 530–537. [\[CrossRef\]](#)
30. Alharthi, F.A.; Alghamdi, A.A.; Alothman, A.A.; Almarhoon, Z.M.; Alsulaiman, M.F.; Al-Zaqri, N. Green synthesis of ZnO nanostructures using *Salvadora Persica* leaf extract: Applications for photocatalytic degradation of methylene blue dye. *Crystals* **2020**, *10*, 441. [\[CrossRef\]](#)
31. Aldeen, T.S.; Mohamed, H.E.A.; Maaza, M. ZnO nanoparticles prepared via a green synthesis approach: Physical properties, photocatalytic and antibacterial activity. *J. Phys. Chem. Solids* **2022**, *160*, 110313. [\[CrossRef\]](#)
32. Mayekar, J.; Dhar, V.; Radha, S. Role of salt precursor in the synthesis of zinc oxide nanoparticles. *Int. J. Res. Eng. Technol.* **2014**, *3*, 43–45.
33. Theivarasu, C.; Indumathi, T. Effect of rare earth metal ion Ce^{3+} on the structural, optical and magnetic properties of ZnO nanoparticles synthesized by the co-precipitation method. *J. Mater. Sci. Mater. Electron.* **2017**, *28*, 3664–3671. [\[CrossRef\]](#)
34. Borysiewicz, M.A. ZnO as a functional material, a review. *Crystals* **2019**, *9*, 505. [\[CrossRef\]](#)
35. Koch, U.; Fojtik, A.; Weller, H.; Henglein, A. Photochemistry of semiconductor colloids. Preparation of extremely small ZnO particles, fluorescence phenomena and size quantization effects. *Chem. Phys. Lett.* **1985**, *122*, 507–510. [\[CrossRef\]](#)
36. Khan, M.M.; Saadah, N.H.; Khan, M.E.; Harunsani, M.H.; Tan, A.L.; Cho, M.H. Potentials of *Costus woodsonii* leaf extract in producing narrow band gap ZnO nanoparticles. *Mater. Sci. Semicond. Process.* **2019**, *91*, 194–200. [\[CrossRef\]](#)
37. Pantidos, N.; Horsfall, L.E. Biological synthesis of metallic nanoparticles by bacteria, fungi and plants. *J. Nanomed. Nanotechnol.* **2014**, *5*, 1. [\[CrossRef\]](#)
38. Ayyanusamy, P.; Alphonse, R.; Minakshi, M.; Sivasubramanian, R. Synthesis of Amorphous Nickel-Cobalt Hydroxides for Ni–Zn Batteries. *Chem. Eur. J.* **2024**, *30*, e202402325. [\[CrossRef\]](#)
39. Minakshi, M.; Samayamanthry, A.; Whale, J.; Aughterson, R.; Shinde, P.A.; Ariga, K.; Kumar Shrestha, L. Phosphorous-containing activated carbon derived from natural honeydew peel powers aqueous supercapacitors. *Chem. Asian J.* **2024**, *19*, e202400622. [\[CrossRef\]](#)
40. Ragunathan, R.; Velusamy, S.; Nallasamy, J.L.; Shanmugamoorthy, M.; Johnney, J.; Veerasamy, S.; Gopalakrishnan, D.; Nithyanandham, M.; Balamoorthy, D.; Velusamy, P. Synthesis and Enhanced Photocatalytic Activity of Zinc Oxide-Based Nanoparticles and Its Antibacterial Activity. *J. Nanomater.* **2022**, *2022*, 3863184. [\[CrossRef\]](#)

41. Álvarez-Chimal, R.; García-Pérez, V.I.; Álvarez-Pérez, M.A.; Arenas-Alatorre, J.Á. Green synthesis of ZnO nanoparticles using a *Dysphania ambrosioides* extract. Structural characterization and antibacterial properties. *Mater. Sci. Eng. C* **2021**, *118*, 111540. [\[CrossRef\]](#)
42. Ameen, S.; Akhtar, M.S.; Nazim, M.; Shin, H.S. Rapid photocatalytic degradation of crystal violet dye over ZnO flower nanomaterials. *Mater. Lett.* **2013**, *96*, 228–232. [\[CrossRef\]](#)
43. Puneetha, J.; Kottam, N.; Rathna, A. Investigation of photocatalytic degradation of crystal violet and its correlation with bandgap in ZnO and ZnO/GO nanohybrid. *Inorg. Chem. Commun.* **2021**, *125*, 108460.
44. Yelpale, A.M.; Patil, V.L.; Bhosale, S.R.; Bhosale, R.R.; Dhavale, R.P.; Vhangutte, P.P.; Kamble, A.J.; Bhange, D.S.; Mane, S.M.; Lee, J.; et al. Efficient photocatalytic degradation of crystal violet dye using time-dependent ZnO nano spindle. *Mater. Sci. Eng. B* **2024**, *310*, 117687. [\[CrossRef\]](#)
45. Ameer, S.B.; Barhoumi, A.; Duponchel, B.; Leroy, G.; Amlouk, M.; Guermazi, H. Physical investigations and photocatalytic activities on ZnO and SnO₂ thin films deposited on flexible polymer substrate. *Vacuum* **2018**, *155*, 546–552. [\[CrossRef\]](#)
46. Kanagamani, K.; Muthukrishnan, P.; Saravanakumar, K.; Shankar, K.; Kathiresan, A. Photocatalytic degradation of environmental perilous gentian violet dye using leucaena-mediated zinc oxide nanoparticle and its anticancer activity. *Rare Met.* **2019**, *38*, 277–286. [\[CrossRef\]](#)
47. Karthik, P.; Ravichandran, S.; Mukkannan, A.; Rajesh, J. Plant-mediated biosynthesis of zinc oxide nanoparticles from *Delonix Elata*: A promising photocatalyst for crystal violet degradation. *Inorg. Chem. Commun.* **2022**, *146*, 110122. [\[CrossRef\]](#)
48. Baral, A.; Das, D.P.; Minakshi, M.; Ghosh, M.K.; Padhi, D.K. Probing environmental remediation of RhB organic dye using α -MnO₂ under visible-light irradiation: Structural, photocatalytic and mineralization studies. *ChemistrySelect* **2016**, *1*, 4277–4285. [\[CrossRef\]](#)
49. Hussien, H.A.J.; Kadhim, R.G.; Hashim, A. Investigating the low cost photodegradation performance against organic Pollutants using CeO₂/MnO₂/polymer blend nanostructures. *Opt. Quantum Electron.* **2022**, *54*, 704. [\[CrossRef\]](#)
50. Sifat, M.; Shin, E.; Schevon, A.; Ramos, H.; Pophali, A.; Jung, H.-J.; Halada, G.; Meng, Y.; Olynik, N.; Sprouster, D.J.; et al. Photocatalytic Degradation of Crystal Violet (CV) Dye over Metal Oxide (MOx) Catalysts. *Catalysts* **2024**, *14*, 377. [\[CrossRef\]](#)
51. Shabna, S.; Singh, C.J.C.; Dhas, S.D.S.J.; Jeyakumar, S.C.; Biju, C.S. An overview of prominent factors influencing the photocatalytic degradation of cationic crystal violet dye employing diverse nanostructured materials. *J. Chem. Technol. Biotechnol.* **2024**, *99*, 1027–1055. [\[CrossRef\]](#)
52. Chen, S.; Liu, Y. Study on the photocatalytic degradation of glyphosate by TiO₂ photocatalyst. *Chemosphere* **2007**, *67*, 1010–1017. [\[CrossRef\]](#) [\[PubMed\]](#)
53. Din, M.I.; Khalid, R.; Najeeb, J.; Hussain, Z. Fundamentals and photocatalysis of methylene blue dye using various nanocatalytic assemblies-a critical review. *J. Clean. Prod.* **2021**, *298*, 126567. [\[CrossRef\]](#)
54. Sakthivel, S.; Neppolian, B.; Shankar, M.V.; Arabindoo, B.; Palanichamy, M.; Murugesan, V. Solar photocatalytic degradation of azo dye: Comparison of photocatalytic efficiency of ZnO and TiO₂. *Sol. Energy Mater. Sol. Cells* **2003**, *77*, 65–82. [\[CrossRef\]](#)
55. Debnath, S.; Ballav, N.; Nyoni, H.; Maity, A.; Pillay, K. Optimization and mechanism elucidation of the catalytic photo-degradation of the dyes Eosin Yellow (EY) and Naphthol blue black (NBB) by a polyaniline-coated titanium dioxide nanocomposite. *Appl. Catal. B Environ.* **2015**, *163*, 330–342. [\[CrossRef\]](#)
56. Ounas, O.; Lekhlif, B.; Jamal-Eddine, J. The facile immobilization of ZnO into a polymer surface for photodegradation of organic contaminants. *Mater. Today Proc.* **2020**, *30*, 816–822. [\[CrossRef\]](#)
57. Flores, N.M.; Pal, U.; Galeazzi, R.; Sandoval, A. Effects of morphology, surface area, and defect content on the photocatalytic dye degradation performance of ZnO nanostructures. *RSC Adv.* **2014**, *4*, 41099–41110. [\[CrossRef\]](#)

Disclaimer/Publisher's Note: The statements, opinions and data contained in all publications are solely those of the individual author(s) and contributor(s) and not of MDPI and/or the editor(s). MDPI and/or the editor(s) disclaim responsibility for any injury to people or property resulting from any ideas, methods, instructions or products referred to in the content.